Critical current studies of a HTS rectangular coil

Z. Zhong,[1] M. Chudy,[2,3] H. S. Ruiz,[4] X. Zhang,[1] and T. Coombs[1]

(1) Department of Engineering, University of Cambridge, UK
(2) Graduate School of Technology Management, University of Pretoria, South Africa
(3) Institute of Power and Applied Electrical Engineering, Slovak University of Technology in Bratislava, Slovak republic
(4) Department of Engineering, University of Leicester, Leicester LE1 7RH, UK

Corresponding author: Michal Chudy (Michal.chudy@stuba.sk)

Abstract

Nowadays, superconducting high field magnets are used in numerous applications due to their superior properties. High temperature superconductors (HTS) are usually used for production of circular pancake or racetrack coils. However different geometries of HTS coils might be required for some specific applications. In this study, the HTS coil wound on a rectangular frame was fully characterized in homogeneous DC background field. The study contains measurements of critical current angular dependencies. The critical current of the entire coil and two selected strands under different magnitudes and orientations of external magnetic fields are measured. The critical regions of the coil in different angular regimes are determined. This study brings better understanding of the in- field performance of HTS coils wound on frames with right-angles.

Keyword: angular dependence, HTS pancake coil, right angle, rectangular frame

1 INTRODUCTION

The high and lossless current-carrying capability of superconductors has been widely recognized. Nowadays, many high-field magnets take advantage of the superior properties of superconductors [1]. To achieve a compact design for superconducting applications, superconductors are wound into different types of coils. Two of the most common coil shapes are pancake coils and racetrack coils. Pancake coils are circular bifilar coils that contain two closely spaced, parallel windings. The name" racetrack" coil arises because at each end the superconductor loops around 180° like the end of a race track. Pancake coils wound using HTS are a viable design option for spatially homogeneous magnets such as NMR and MRI magnets [2,3]. Racetrack coils, on the other hand, are preferred in generators [4], motors [5] and maglev systems [6].

Most superconducting coil based applications involve external magnetic fields or background fields, which are large enough to significantly affect the critical current of a superconducting coil. In addition, the anisotropic nature of superconducting tape has a great impact on the in field performance of superconducting coils. Many numerical methods have been proposed to study the behavior of superconducting coils. Critical regions and subcritical regions were assumed by J.R. Clem [7], depending on the magnetic environment. W. Yuan [8] predicted the boundary between these two regions by using a parabolic function and calculated the current distribution within the subcritical regions. V.M.R. Zermeno [9] made a further step towards efficient modelling by devising a 3D approach.

Some experimental studies have also been carried out. The field angular dependence of a racetrack coil has been measured, in which the critical current variation showed a good agreement with that of a single tape [10]. The critical current for different radial parts (from inner sections to outer sections) of a pancake coil has also been measured, suggesting that the inner layers contribute much more to the resulting end-to-end voltage drop than the outer

layers do, when the applied current is greater than a critical value. This could jeopardize the smooth operation of a superconducting coil. As a result, more adequate criteria for determining the critical current of a superconducting coil was proposed [11].

Rapid developments have been made in superconducting coil fabrication processes and technology [12]. Initially, the dry winding technique was widely used, which wound superconducting coil without any filler material. The main drawback of this technique is the motion and friction of the conductor within the coil windings caused by the Lorentz force, even though global winding motions can be controlled over a macroscopic scale by mechanical reinforcement. However, the heat generated by conductor motion can be effectively taken away by cryogenic coolant irrigation of the porous windings [13]. Coil based superconductors can therefore be safely used for most purposes [14]. Impregnation of coil windings with filler materials is an alternative approach. The material fills the winding voids and thereby prevents the Lorentz force-induced conductor motion. Materials with low moduli of elasticity have been used and evaluated as impregnates, and epoxy resin was proven to be the most successful candidate. However, this is by no means a flawless solution, as the critical current of an epoxy-impregnated YBCO coil can be substantially degraded [15,16]. Currently there is no standard way of producing superconducting coils and the most desired solution is usually realized based on case-specific analysis. Recently, a new type of superconducting coils, the square coil, has aroused great interest. For a Helmholtz coil, they have been proven to be better candidates than circular windings in generating a more uniform magnetic field [17]. However, this geometry also results in a concentration of the coil self-field in certain regions. Investigation into the field distribution is required. The situation becomes even more complicated if a square coil is in the presence of an external magnetic field. At present, few studies have been done with respect to a square or rectangular superconducting coils. A deep insight into the factors that determine the critical current of such coils would be extremely beneficial.

Some extra care needs to be taken while fabricating superconducting coils on frames with right angles. Firstly, the corners must be made slightly circular with a diameter greater than that of the minimum bending diameter of the winding tapes. Secondly, as superconductor wires pass around a corner, the tape cannot easily be bound to the straight parts of the frame. Gaps are more likely to exist between the inner-most layer of the coil windings and the frame. This gap, although small, could still have a large in influence on the overall performance of the coil.

In this paper the field angular dependence of the critical current for two selected sections of a rectangular coil as well as for the entire coil is measured. The effect of flux cutting and flux transport (de-pinning) on the critical current of selected sections and the entire coil are discussed. The effects of mechanical disturbance induced by the small gaps are investigated. The critical region that dominates the overall critical current of the coil is identified in different angular regimes.

2. EXPERIMENTAL PROCEDURE

2.1 Test Coil

The rectangular coil was wound using Superpower® SCS6050 tape [18], which is a double stack rectangular-shaped 2G HTS coil. Kapton® tapes were used as electrical isolation between turns. The dimensions of the coil are illustrated in Fig. 1a. Several parameters of the superconducting coil are collected in Table 1.

Voltage taps were soldered to the terminals at each end of the coil to evaluate the critical current of the entire coil. Three additional voltage taps (V1, V2, and V3) were also soldered to the straight portion and corner portion of the innermost layer, spacing 25 mm from each other, to determine the critical current of the corresponding strands (Fig. 1). The straight strand, where voltage taps V2 and V3 were accommodated, was not bound to the frame. The maximum distance between the innermost layer of the straight strand and the frame was measured to be 1.4 mm. Windings in other regions were bound to the G10 frame using Kapton ^{R} tapes.

Table 1: Parameters of the superconducting coil

Tape type	Superpower ® SCS6050 (2013)
Tape width	6 mm
Tape thickness	100 m
Substrate	50 m Hastelloy ^{R} C-27, non-magnetic
Number of turns	32 turns per layer (two layers)
Length	16.6 m

The coil was mounted on a tufnol support board, together with all the sensors and instrument wires. Each terminal was connected to the current lead by clamping it between two copper plates. A Hall probe was placed at the centre of the coil to monitor the magnitude of the magnetic fields.

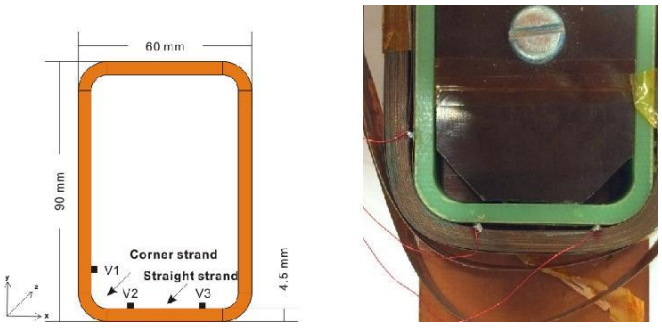

(a) Dimension drawing of the rectangular coil.

(b) Picture of the rectangular coil.

Fig. 1: Dimension drawing and picture of the rectangular coil. It can be seen in Fig. 1b that a small gap exists between the innermost layer of the straight strand and the G10 frame.

2.2 Experimental set-up

A schematic drawing of the experimental set-up is dis-played in Fig. 2. Transport I_c measurements of the entire coil and selected sections were performed using a four-probe technique and an electric field criterion of E_0=1x10 $^{-4}$ V/m. The coil was completely immersed in a liquid nitrogen bath. The applied current was ramped up at 2 A.s $^{-1}$ to reduce the impact of inductance inside the coil. Angular studies were performed in an electro-magnet with a field homogeneity of 8% ppm in the region where the test coil was placed. The maximum achievable field is 330 mT for this air-gap. The magnetic field was monitored by a Hall sensor placed at the centre. The coil was rotated by a high precision manual rotation stage (graduation of 1 and vernier of 5') around a vertical axis. An Agilent 6680A was used as the current source and two Keithley 2182 nanovoltmeters were employed to monitor the voltage signals of the entire coil as well as the selected sections. The measurements were controlled using a LabVIEW platform.

3. RESULTS AND DISCUSSION

The critical current measurement in the self-field condition was first performed, giving a critical current of 66 A for the entire coil, 63 A for the straight strand and 58 A for the corner strand, respectively. The second innermost layer was chosen for characterization as the innermost layer contains a crossover of the tapes between the windings. The I_c of the coil was higher than for the innermost strands. This occurs because I_c is determined

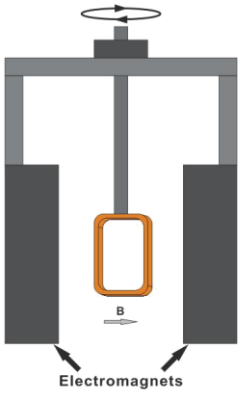

Fig. 2: Experimental Set-up

as being when $E>E_0$. When $E>E_0$ for the entire coil, the electric field (E) of the innermost strands is considerably higher than E_0[11]. The variation of the critical currents in different regions could be attributed to either one or both of the effects of the inhomogeneous field distribution and different mechanical conditions experienced by the straight and corner strands. These two factors are discussed in sections 3.1 and 3.2.

The critical current was then measured in the presence of external magnetic fields with various magnitudes. The angle between **H** and the coil is defined as $\theta_{coil} = 0°$ when the external field is perpendicular to the x-y plane (see Fig. 1a), and the coil was rotated clockwise around the y axis with an interval of 4 degrees. The critical current of either the corner strand or straight strand could not be determined under all conditions, such as the angular regions that are close to 0 under higher external magnetic fields. This is due to the protection mechanism applied. The transport current was regulated to zero when a pre-set threshold voltage for the entire coil (6 mV) was exceeded, while the voltages of either corner and straight strands remained well below the criteria voltage V_c of 2.5 μV .

3.1 Inhomogeneous magnetic field distribution

Superconducting strands in the innermost layer tend to experience the highest density of the magnetic self-field generated by the coil, and therefore are penetrated more by the critical regions compared to the outer turns, leading to a lower critical current [19]. Unlike circular-shape pancake coils, where each layer of a superconducting coil experiences a similar magnetic field condition, every single part of a rectangular-shaped coil, can experience different densities and orientations of magnetic fields. Due to the effects of geometry, the corners of the innermost layer are in the presence of the strongest field in self-field conditions. A Comsol model (Fig. 3) using E-J characterization of the tape shows that the corner regions and inner layers experience stronger magnetic fields than the straight portions and outer layers. A peak magnetic flux density of 0.24 T is present at one corner of the innermost layer, while a minimum of 0.129 T is seen at one corner of the outermost later when an external current of 69 A is applied. The average flux density along the straight strands is smaller than that of the corner strands in each layer. This could be due to the field superposition at the corner regions. Thus, a lower critical current is expected at the corner strand than in the straight strand in the self-field condition.

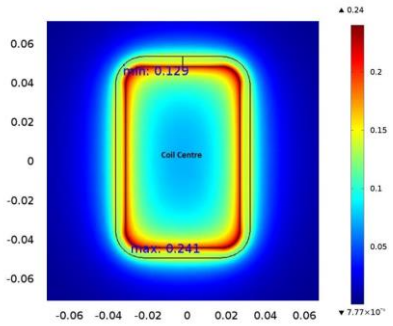

Fig. 3. Resulting magnetic flux density (T) from Comsol model of the coil. The center-cut plane of the coil is modelled, when an external current of 66 A is applied. AC/DC Module, Magnetic field(mf) is used for the simulation and Multi-turn Coil is used for current injection

The situation becomes more complicated when an external magnetic field is applied. In this case, the field distribution is more complex because of the vector superposition of the applied magnetic fields and the self-field generated by the coil. The strongest magnetic field may occur in any region in a given field orientation and magnitude. The peak field is no longer confined to the innermost layer, nor to any other specific region. The field distribution changes greatly as the orientation of the applied fields varies. Another important issue which needs to be addressed is the field orientation. Different field angles are defined depending on the direction of the rotation: the tilt angle and the rotation angle. The definition of these two angles is illustrated in Fig. 4. θ_{coil} is defined as 0° when $H \parallel c$ axis, and 90° when $H \parallel ab$ plane. φ is defined as 0° when the sample is subject to the maximum Lorentz force configuration, and 90° when the sample is a subject to the minimal Lorentz force configuration (i.e.

the applied field is parallel to the current direction.). When the coil is rotated around the y axis as shown in Fig. 5, the superconducting strands in the straight part A (coloured in blue) are always in the maximal Lorentz force configuration, in which the orientation of the applied magnetic field is always perpendicular to the current direction. A characteristic curve for the angular dependence of the critical current on the applied magnetic field was obtained for SuperPower samples (Fig. 6).

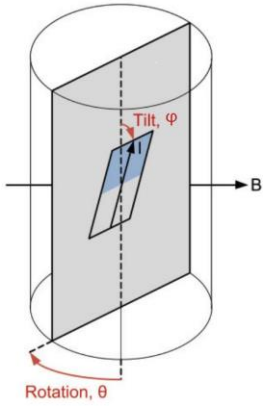

Fig.4. Definitions of the rotation angle (θ) and the tilt angle (φ).

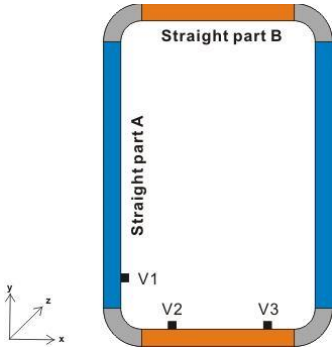

Fig. 5. The coil is divided into three parts depending on various field conditions experienced. The y-axis runs through the centre of the coil.

A different situation occurs for the straight part B (colored in orange Fig. 5). In these parts, the superconducting strands experience an in-plane magnetic field (the x-z plane as shown in Fig. 5). During rotation, it is expected that B_z will not have a great influence on the critical current, due to the strong intrinsic pinning arising from the layered structure. B_x, on the other hand, is parallel to the current direction. The enhancement of the critical current caused by this parallel component of an applied magnetic field has been observed [22-24]. Flux cutting is believed to be responsible for this enhancement [25, 26]. A general critical state model(GCSM) that could describe this phenomenon was firstly proposed by Clem [27,28], which takes into account both vortex motions induced by transverse current and vortex twist caused by longitudinal currents. This model is purely phenomenological. Campbell [29] admits that “we are a long way from even a qualitative understanding of flux cutting and longitudinal currents." The intricate flux cutting theory will therefore not be explored in this paper, instead, we focus on the enhancement of critical current of a superconducting strand when it is in the presence of longitudinal applied fields, and the effects on the entire rectangular coil. The critical current dependence of a superconducting tape on in-plane applied fields has been studied previously [20, 24]. It can be seen from Fig. 7a that the critical current is not sensitive to a moderate tilt angle ($\varphi < 45°$), whilst increases remarkably at higher tilt angles. The peaks are seen at $\varphi = 90$ (force-free configuration) when the applied field is perpendicular to the sample surface ($H \parallel c$). The critical current remains level with the variation in tilt angle when the applied field is parallel to the sample surface, where **H** is always parallel to the ab plane and perpendicular to **I**. The magnetic field component is perpendicular to the current direction therefore does not exert a great influence on the performance of the critical current.

The fan-shaped corner strand (colored in grey in Fig. 5), experiences various tilt angles in a broad range of tilt angles from 0° to 90° at certain rotation angles. Fig. 7b shows the I_c variations depending on both rotation angle and the tilt angle. When the tilt angle is smaller than 45°, the rotation angle determines the critical current. Only a minute I_c enhancement is observed, whereas the value of the sharp maximum seen at a rotation angle of 90° remains unchanged. As the applied field progressively tilts to a direction aligned to the direction of current I, a pronounced I_c enhancement is achieved for all rotation angles apart from 90° and 270°. A completely different tendency is seen in the critical current profiles when φ = 90°. This occurs when an in-plane field is applied to the sample, so that the rotation angle θ essentially represents the angle between **B** and **I**. A minimum is seen when **B** $\perp$ **I**, while a maximum is seen when **B** $\parallel$ **I**.

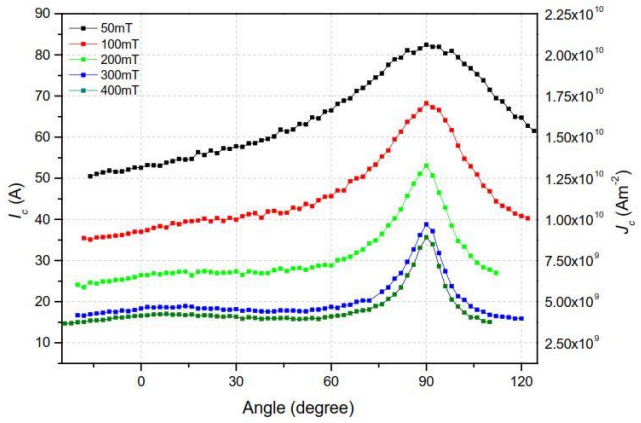

Fig. 6. Critical current of 4 mm wide Superpower® samples as a function of magnetic field orientations at 77 K. 0° is defined as when the applied field is perpendicular to the broad surface of the sample, and defined as 90° when the applied field is parallel to the broad surface of the sample.

3.2 Mechanical strain and conductor motions

The interaction between magnetic fields and transport current causes a variation in the Lorentz force exerted on different superconducting strands. This force generally leads to tensile strain, which can influence performance of a superconductor [30 -32]. Investigations into the relationship between the critical current and strain/stress have been done by Hyung-Seop Shin [33], and show that I_c experiences a slight increase, reaching a peak at a strain of $\varepsilon_{irr:}$=0.25%. I_c begins to degrade rapidly with a further increase in strain. The critical axial tensile stress reported by the manufacturer is 4.5% [18], which is far beyond the tensile stress experienced by the measured coil. Thus, the effect of tensile strain is negligible. Another type of deformation is bending, which also leads to I_c degradation [34]. However, the bend diameter for this coil is (24 mm), which is substantially larger than the critical tensile bend diameter (11 mm) reported by the manufacturer [18]. Therefore, no I_c reduction for this reason should be present.

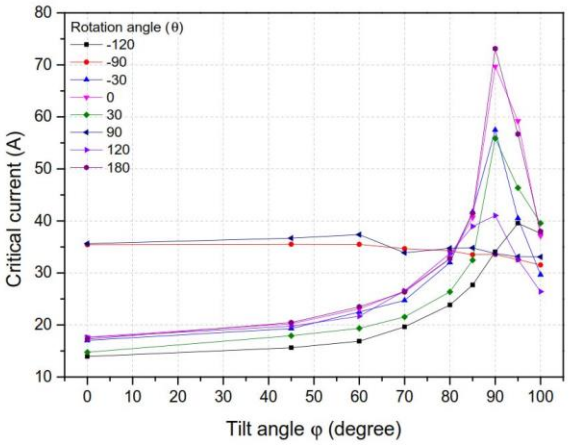

(a) Critical current vs. tilt angles (φ).

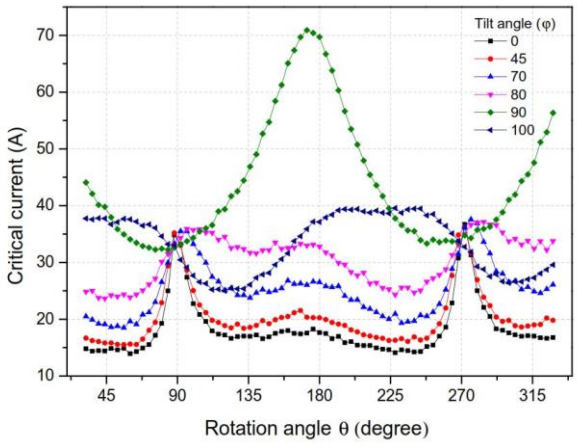

(b) Critical current vs. rotation angles (θ).

Fig. 7. Two-axis orientation dependent critical current measurements on a SuperPower® sample. The conductor was subjected to an applied magnetic field of 500 mT.

The air gap between the innermost layer of the straight part B and the G10 support frame (Fig. 1b and Fig. 8) can have a deep influence on the critical current of corresponding strands in the presence of external magnetic fields. The air gap either expands or contracts due to the Lorentz force - F_l , which can be calculated:

$$\mathbf{F_l} = I \int dl \times \mathrm{B} \qquad (1)$$

The average force exerted on the 25 mm long straight strand (innermost layer) is estimated by a simulation performed by Comsol 4.4b. The results are presented in Fig. 9. The direction of the self-field is opposite to the direction of the applied field at $\theta_{coil} = 0°$. This is defined as positive when the resulting Lorentz force is in the -y direction as illustrated in Fig. 5. Fig. 9 shows that at $\theta_{coil} = 135°$ and $\theta_{coil} = 225°$, the straight strand experiences approximately the same force in the y direction under different magnitudes of applied magnetic field. Therefore, similar conductor movement is expected for the strand at these two coil rotation angles for different applied fields. As the bottom straight part B was left loose, the magnitude of the Lorentz force is sufficient to push the strands upwards in the +y direction, especially in the presence of strong fields (200 mT, 300 mT).

Fig. 8. Schematic illustration for the bottom section of the measured rectangular coil (refer to Fig. 1b). The maximum distance between the innermost layer of straight part B and the G10 support frame is 1.4 mm.α is estimated to be 6

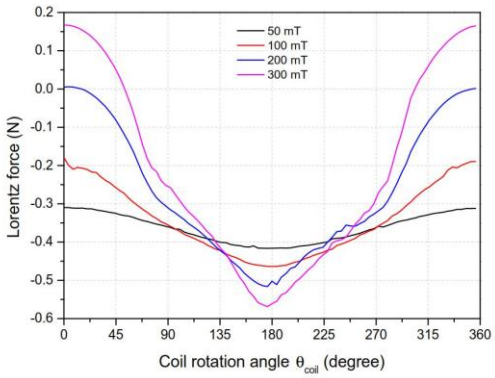

Fig.9. Simulation results for the Lorentz force exerted on the 25 mm long straight strand (innermost layer).

Therefore, the x component of the applied field (B_x) is no longer always aligned with the current direction (**I**). Instead, there is a slight tilt between B_x and **I**, with various angles over different regions of the curved strands. Although the tilt angles are small (<10°), they tend to affect the critical current significantly (Fig. 7b). According to Fig 4, **B** is an in-plane applied field when tilt angle φ = 90°. Fig. 7b shows that the critical current of a single tape is extremely sensitive to a slight `off-plane' tilt. A completely different picture is seen for φ = 80° and φ = 100° compared to φ = 90°. It is essentially the case for the left half and right half of the straight part B (Fig. 8). Either the left half or the right half could be the critical region for the straight part B, depending on the coil rotation angle (θ_{coil}), and determine the critical current for the entire strand.

3.3 Critical current for different sections of the measured rectangular coil

Critical currents for the straight strand (straight part B), the corner strand and the entire coil were measured under four different magnitudes of applied magnetic fields: 50 mT, 100 mT, 200 mT, and 300 mT. Applied field magnitudes could be distinguished into three levels: moderate fields where the applied field is smaller than the coil self-field (e.g., 50 mT); intermediate fields where the applied field is comparable to the coil self-field (e.g., 100 mT); and strong fields where the applied field is greater than double value of the self-field (e.g., 200 mT and 300 mT). The critical current profiles are presented in Fig. 10. As the critical current of the entire coil was evaluated using the end-to-end voltage, it is essentially the overall average for each part of the coil. Therefore, some parts or layers can contribute more to the resulting end-to-end voltage than others. In this case the corresponding part or layer becomes the predominant factor in determining the critical current of the entire coil.

In this paragraph, critical regions for the sample coil are identified in the presence of rotating external magnetic field. As mentioned previously, the coil is divided into three parts (Fig. 5). It is expected that a given part within each superconducting layer experiences a similar field orientation but varying field magnitudes. The innermost layer of a part can probably serve as a representative to study the critical current tendency of the corresponding part. During experiments, the rectangular coil was rotated around the y-axis, and the rotation angle of the coil (θ_{coil}) is defined as 0° when the applied field is perpendicular to the x-y plane (Fig. 5). Thus, the applied field is perpendicular

to the ab-plane of the superconducting strands in the straight part A when $\theta_{coil} = 0°$, and is an in-plane applied field with $\mathbf{B} \perp \mathbf{I}$ for the straight part B.

The critical current variation of the straight strand (bottom straight part B) decreases monotonically as the applied field progressively tilts towards the direction of the current. The minimum is reached at 135°. Then the critical current experiences a gentle increase for all the remaining angular regions when 50 mT external field is applied (Fig 10a). For intermediate and strong fields, the critical current begins to decrease after reaching a smaller peak at $\theta_{coil} = 180°$, arriving at another minimum at 225° (Fig. 10b, Fig. 10c and Fig. 10d), and rising again with increasing θ_{coil}. Although this is rather surprising behavior. According to physics, If the straight strand is closely bonded to the frame, the applied field is always in-plane, the critical current is expected to reach peaks at 90° and 270° where **B** is aligned with **I**, and reach minima at 0°, 180°, when **B** is perpendicular to **I** [23,18]. However, this straight strand is not tightly bound, and creates a small gap between the straight strand and the G10 frame (Fig. 1b). This straight strand is slightly curved and experiences a small `off-plane' tilt field instead. Fig. 10 shows that this small conductor motion has a great impact on the resulting critical current curve. As shown in Fig. 9, the Lorentz force on the straight strand is approximately the same under applied fields of different magnitudes at $\theta_{coil} = 135°$ and $\theta_{coil} = 225°$, suggesting similar conductor movement. The minima positions for the straight strand are possibly resulting from the joint action of conductor motion and `tilting' to the applied magnetic fields. However, the wire motions are expected to be rather insignificant for the entire straight part B as all the other parts are tightly bonded to the frame.

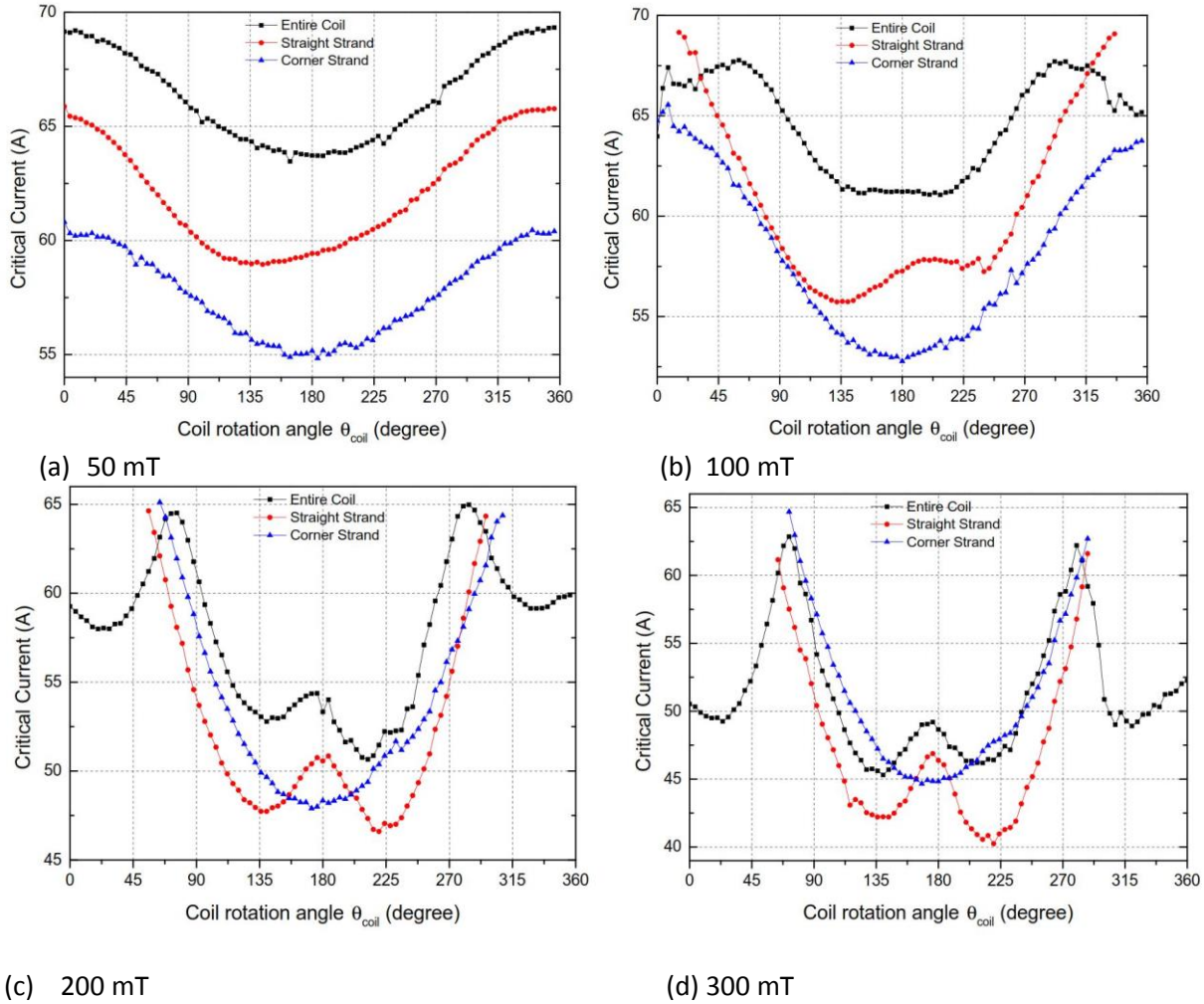

Fig. 10. Critical current for the corner strand, the straight strand, and the entire coil under various field magnitudes and orientations.

Fig 10a shows that the critical current variation of the corner strand and the entire coil are identical under 50 mT external magnetic field, suggesting that the corner areas are the critical region for all rotation angles under moderate fields (50 mT). This could be due to the fact that the self-field of the superconducting coil is concentrated

in the corner regions, whereas the applied field is too small to become the major factor. When the applied field is 100 mT, in the region of 135° < θ_{coil} <225°, the critical current of the entire coil remains at a value, which may originate from compensation between the straight strand and the corner strand. The straight part A is not considered to play the important role in the determination of the overall critical current, as the critical current variation is expected to be only moderate (Fig. 6). The situation is different when the stronger fields are applied. (200 mT and 300 mT) Here the straight strand dominates in determination of the overall critical current of the coil. The crossings between the critical current of the straight strand, the corner strand and the entire coil indicates that for θ_{coil} < 80° and θ_{coil} > 280° , the studied layer is no longer the critical region in determining the overall critical current under strong fields.

Fig. 11 shows the critical current variation of the entire coil. As discussed before, the overall critical current is mainly determined by the corner part when the applied field is low (50 mT and 100 mT). However, in the case of a strong applied field, straight part A and straight part B turn into the major factors. The straight part B as a whole is not expected to be significantly affected by the wire motion since all the other parts of the wire are reinforced. The in-plane applied magnetic field is therefore considered to be the primary factor in determining the critical current for the whole part. The critical current variation of each part with respect to field orientation should be similar to that of a single tape. Fig. 12 presents a schematic diagram showing the expected tendency of critical current for the straight part A and the straight part B. When θ_{coil} = 0° , the applied field, B_{app} is in the *z* direction when the current flows in the x-y plane (Fig. 13).

Fig. 12 shows that the critical current decreases much faster in the angular regime 0°< θ_{coil} <45° than in 45°< θ_{coil} < 90° for the straight part A. For the straight part B, the critical current increases more rapidly in the angular regime 45°< θ_{coil} <90° than in 0° < θ_{coil} <45°. The changing slope of the critical current over different angular regimes leads to the presence of multiple peaks and minima for the critical current of the entire coil (Fig 12). The critical current reduction for the straight part A is much greater than the increase for the straight part B for 0 < θ_{coil} <45°, and therefore the critical current for the entire coil is reduced. For the angular regime 45°< θ_{coil} <90°, the large critical current increase in the straight part B and slight decrease in the straight part A result in increased critical current of the entire coil. A similar explanation applies to all the remaining angular regimes.

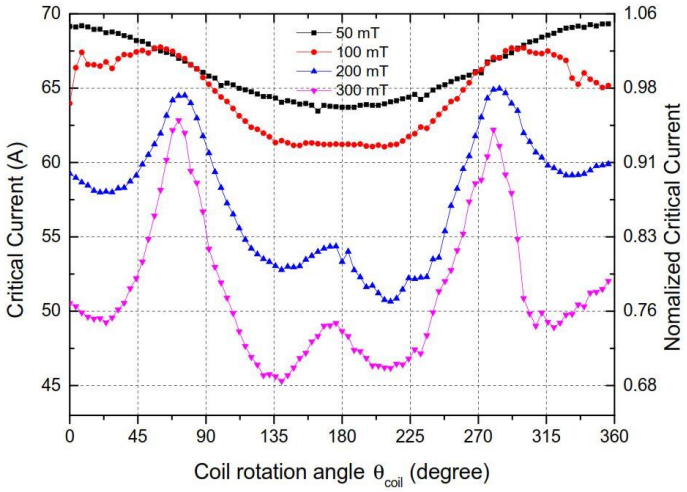

Fig. 11. Critical current of the entire coil subjected to different external fields. I_c is normalized to the self-field values to better demonstrate the comparison.

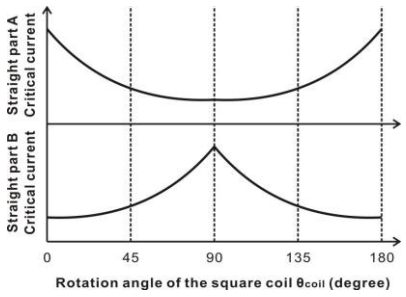

Fig.12. Expected trends of critical currents for the straight part A and the straight part B according to the experiments performed on a single tape. The tendency was estimated according to the experimental results from a single tape (Fig. 6 and Fig, 7a).

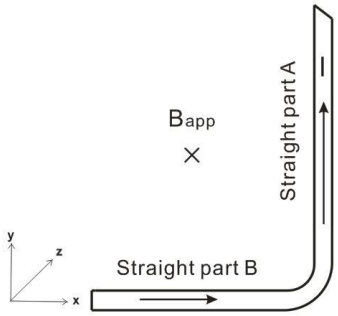

Fig. 13. Illustration of the current and field directions for the coil at $\theta_{coil} = 0°$. The cross indicates that the applied field is in the *z* direction. The arrows indicate the direction of the current.

To conclude, the dominant factor for determination of critical current in strong fields is: the straight part A when $0° < \theta_{coil} < 45°$, $135° < \theta_{coil} < 225°$ and $315° < \theta_{coil} < 360°$. And the straight part B when $45° < \theta_{coil} < 135°$ and $225° < \theta_{coil} < 315°$.

The critical current of the entire coil was determined using the end-to-end voltage, which is essentially the integration of the electric field over the length of the sample. The straight part A (80 mm) is longer than straight part B (50 mm), and therefore contributes more to the end-to-end voltage, providing that a similar electric field is experienced by both parts. This is the reason why the peaks and minima shown shifts (Fig.11) to the angular regimes where the critical current of the straight part A experiences a rapid increase or decrease

4. CONCLUSION

Critical current performance of the coil wound on the rectangular frame in magnetic field was studied. The critical currents of the entire coil and two selected strands under different magnitudes and orientations of external magnetic field were acquired. It was shown that a small gap between the innermost layer and the frame of the coil can have a huge impact on the critical currents. Therefore, it is advisable to impregnate similar coils to reduce wire motions. Corner regions are considered to be the critical region for such coils in the presence of a small or intermediate external magnetic field, the magnitude of which is smaller or comparable to the self-field generated at the centre of the coil. In the case of a strong magnetic field, either the straight part A (longer portion) or the straight part B(shorter portion) can become the dominant factor for the critical current determination of the entire coil in certain angular regimes.

REFERENCES

[1] A. M. Asner, High field superconducting magnets (Clarendon Press, 1999).

[2] J. Bascunan, H. Lee, E. S. Bobrov, and Y. Iwasa, “A low-and high-temperature superconducting nmr magnet: Design and performance results," Applied Superconductivity, IEEE Transactions on 13, 1550 - 1553 (2003).

[3] B. C. Breneman, R. E. Sarwinski, and Y.-H. L. Hsu, “Superconducting mri magnet with magnetic flux field homogeneity control," (1993), uS Patent 5,194,810.

[4] H. Wen, W. Bailey, K. Goddard, M. Al-Mosawi, C. Beduz, and Y. Yang, “Performance test of a 100 kw hts generator operating at 67 k-77 k," Applied Superconductivity, IEEE Transactions on 19, 1652-1655 (2009).

[5] Z. Huang, W. Xian, M. Zhang, M. Chudy, Y. Chen, Z. Zhong, M. Baghdadi, W. Wang, F. Spaven, K. Matsuda, et al., “Control and operation of a high temperature superconducting synchronous motor," Applied Superconductivity, IEEE Transactions on 23, 5200204 (2013).

[6] K. Tasaki, K. Marukawa, S. Hanai, T. Tosaka, T. Kuriyama, T. Yamashita, Y. Yanase, M. Yamaji, H. Nakao, M. Igarashi, et al., “Hts magnet for maglev applications (1) coil characteristics," Applied Superconductivity, IEEE Transactions on 16, 1100-1103 (2006).

[7] J. R. Clem, J. Claassen, and Y. Mawatari, “AC losses in a finite z stack using an anisotropic homogeneous-medium approximation," Supercond. Sci. Technol. 20, 1130 (2007).

[8] W. Yuan, T. Coombs, J.-H. Kim, C. H. Kim, J. Kvitkovic, and S. Pamidi, “Measurements and calculations of transport ac loss in second generation high temperature superconducting pancake coils," Journal of Applied Physics 110, 113906 (2011).

[9] V. M. Zermeno and F. Grilli, ”3-d modeling and simulation of 2g hts stacks and coils," arXiv preprint arXiv:1311.3580 (2013).

[10] M. Chudy, Y. Chen, M. Zhang, and T. Coombs, “Anisotropy of 2g hts racetrack coils in external magnetic fields," Supercond. Sci. Technol. 26, 075012 (2013).

[11] M. Zhang, J.-H. Kim, S. Pamidi, M. Chudy, W. Yuan, and T. Coombs, “Study of second generation, high-temperature superconducting coils: Determination of critical current," Journal of Applied Physics 111, 083902 (2012).

[12] Y. Iwasa, Case studies in superconducting magnets: design and operational issues (Springer, 2009).

[13] J. Williams, “High current density superconducting coils," Tech. Rep. (Massachusetts Inst. of Tech., Cambridge (USA). National Magnet Lab., 1967).

[14] Y. Iwasa, “Experimental and theoretical investigation of mechanical disturbances in epoxy-impregnated superconducting coils”. 1. general introduction," Cryogenics 25, 304-306 (1985).

[15] T. Takematsu, R. Hu, T. Takao, Y. Yanagisawa, H. Nakagome, D. Uglietti, T. Kiyoshi, M. Takahashi, and H. Maeda, “Degradation of the performance of a ybco-coated conductor double pancake coil due to epoxy impregnation," Physica C 470, 674-677 (2010).

[16] D. Van Der Laan, J. Ekin, C. Clickner, and T. Stau er, “Delamination strength of ybco coated conductors under transverse tensile stress," Supercond. Sci. Technol. 20, 765 (2007).

[17] U. Prasad, A. Amardas, D. Patel, S. Pradhan, et al., “Design and fabrication of a high t_c bscco based square helmholtz coil," Journal of Physics: Conference Series, Vol. 208 (IOP Publishing, 2010) p. 012021.

[18] http://www.superpower-inc.com/, (2013).

[19] M. Zhang, J. Kvitkovic, C. Kim, S. Pamidi, and T. Combs, “Study of 2g high temperature superconducting coils: Influence of anisotropic characteristics," Journal of Applied Physics 114, 043901 (2013).

[20] S. Hopkins, M. Wozniak, B. Glowacki, Y. Chen, I. Kesgin, and V. Selvamanickam, “Two-axis magnetic field orientation dependence of critical current in full-width rebco coated conductors," Physics Procedia 36, 582- 587 (2012).

[21] M. Chudy, Z. Zhong, M. Eisterer, and T. Coombs, “n-values of commercial ybco tapes before and after irradiation by fast neutrons," Supercond. Sci. Technol. 28, 035008 (2015).

[22] E. H. Brandt and G. Mikitik, “Longitudinal magnetic field increases critical current in superconducting strip," Journal of Physics: Conference Series, Vol. 150 (IOP Publishing, 2009) p. 052024.

[23] G. P. Mikitik and E. H. Brandt, “Vortex shaking in rectangular superconducting platelets," Phys. Rev. B 69, 134521 (2004).

[24] M. Chudy, S. Hopkins, M. Wozniak, B. Glowacki, M. Eisterer, and H. Weber, “Full angular critical current characteristics of coated conductors studied using a two-axis high current goniometer," Supercond. Sci. Technol. 24, 075018 (2011).

[25] V. Vlasko-Vlasov, A. Koshelev, A. Glatz, C. Phillips, U. Welp, and W. Kwok, “Flux cutting in high-t_c superconductors," Physical Review B 91, 014516 (2015).

[26] L. Fisher, K. Il'enko, A. Kalinov, M. LeBlanc, F. Perez-Rodriguez, S. Savel'ev, I. Voloshin, and V. Yampol'skii, “Suppression of the magnetic moment under the action of a transverse magnetic field in hard superconductors," Phys. Rev. B 61, 15382 (2000).

[27] J. R. Clem, “Flux-line-cutting losses in type-slowromancapii@ superconductors," Phys. Rev. B 26, 2463 (1982).

[28] J. R. Clem, M. Weigand, J. Durrell, and A. Campbell, “Theory and experiment testing flux-line cutting physics," Supercond. Sci. Technol. 24, 062002 (2011).

[29] A. Campbell, “Flux cutting in superconductors," Supercond. Sci. and Technol 24, 091001 (2011).

[30] J. Yoo and D. Youm, “Tensile stress effects on critical current densities of coated conductors," Supercond. Sci. Technol 14, 109 (2001).

[31] C. Park, D. Norton, J. Budai, D. Christen, D. Verebelyi, R. Feen-stra, D. Lee, A. Goyal, D. Kroeger, and M. Paranthaman, “Bend strain tolerance of critical currents for yba_2 cu_3o_7 films deposited on rolled-textured (001) ni," Appl. Phys. Lett. 73, 1904 -1906 (1998).

[32] J Emhofer, M Eisterer and H W Weber, “Stress dependence of the critical currents in neutron irradiated (RE)BCO coated conductors”, Supercond. Sci. Technol. 26, 035009 (2013).

[33] H.-S. Shin, K.-H. Kim, J. R. C. Dizon, T.-Y. Kim, R.-K. Ko, and S.-S. Oh, “The strain effect on critical current in ybco coated conductors with different stabilizing layers," Supercond. Sci. Technol. 18, S364 (2005).

[34] R. Champailler, N. Yanagi, G. Bansal, H. Tamura, T. Mito, S. Imagawa, and J.-L. Duchateau, ‘Experiments of bending strain on reduced-scale hts conductors for fusion energy reactors," Applied Superconductivity, IEEE Transactions on 20, 1565-1568 (2010).